SCIENCE CHINA
Information Sciences

• RESEARCH PAPER •

April 2026, Vol. 69, Iss. 4, 142402:1–142402:8
https://doi.org/10.1007/s11432-025-4600-y

# Unveiling in-plane and out-of-plane phonon anisotropy in $NbIrTe_4$ through polarization-resolved Raman spectroscopy

Ting WEN[1†], Yalan WANG[2†], Shuang CAI[2†], Ziluo SU[2†], Jiaqi WU[2], Jiaze QIN[2], Chenyin JIAO[2], Zejuan ZHANG[2*], Zenghui WANG[2*] & Shenghai PEI[2*]

[1]*School of Electronic Information, Huzhou College, Huzhou 313000, China*
[2]*Institute of Fundamental and Frontier Sciences, University of Electronic Science and Technology of China, Chengdu 610054, China*

Received 17 June 2025/Revised 20 August 2025/Accepted 16 September 2025/Published online 3 February 2026

**Abstract** $NbIrTe_4$, a low-symmetry layered material, exhibits pronounced anisotropic electronic and vibrational properties, making it a compelling platform for anisotropic and topological applications. However, its Raman-active phonon modes remain partially undiscovered, due to selection rule limitations in conventional configurations. In this study, we employ angle-resolved polarization Raman spectroscopy to comprehensively probe both in-plane and out-of-plane phonon modes, enabling the full revelation of all Raman-active modes, including the out-of-plane $B_1$ and $B_2$ modes that we observe experimentally. By analyzing polarization-dependent spectra across multiple orientations, we uncover strong anisotropy in phonon behavior and extract Raman tensor components. These findings advance the fundamental understanding of direction-dependent vibrational dynamics in $NbIrTe_4$ and offer a theoretical foundation for exploring orientation-tunable properties in low-symmetry 2D materials.

**Keywords** out-of-plane, $NbIrTe_4$, anisotropy, polarization-resolved Raman spectroscopy, 2D materials

**Citation** Wen T, Wang Y L, Cai S, et al. Unveiling in-plane and out-of-plane phonon anisotropy in $NbIrTe_4$ through polarization-resolved Raman spectroscopy. Sci China Inf Sci, 2026, 69(4): 142402, https://doi.org/10.1007/s11432-025-4600-y

## 1 Introduction

$NbIrTe_4$, a low-symmetry layered material, exhibits strong anisotropic electronic and vibrational properties, making it a promising candidate for future topological and sensing applications [1, 2]. Interesting, it has a topological nature [3, 4], which is not readily available in some other anisotropic 2D materials such as black phosphorus and $ReS_2$, making it a unique platform for exploring anisotropic topological features. Its unique crystal structure gives rise to complex phonon behaviors and strong electron-phonon interactions, which are essential for understanding its fundamental physical properties [5, 6]. A detailed investigation of these phonon characteristics would be necessary to provide critical insights into interlayer coupling, symmetry-dependent vibrational modes, and modulation effects from external fields.

Given the highly anisotropic nature of $NbIrTe_4$, its vibrational properties require experiments capable of resolving direction-dependent phonon responses with high precision [7]. Polarization-resolved Raman spectroscopy is particularly suited for this purpose [5], as it enables selective excitation and detection of vibrational modes according to Raman selection rules [8, 9]. By precisely controlling the polarization of incident and scattered light, it becomes possible to distinguish in-plane and out-of-plane phonon modes, thereby probing the symmetry characteristics and anisotropic phonon behavior in a crystal [10]. Additionally, this technique can provide insight into electron-phonon interactions and their responses to external stimuli [5, 11].

However, despite these advantages, the Raman-active phonon modes of $NbIrTe_4$ remain yet to be fully characterized, hindering further understanding of its vibrational properties and electron-phonon interactions. This is because in low-symmetry 2D materials, selection rule constraints often prevent the observation of certain modes under standard measurement configurations, resulting in incomplete phonon spectra [12, 13]. Overcoming this limitation requires optimizing experimental parameters to enable comprehensive phonon mode detection, such as laser

* Corresponding author (email: zejuanzhang@uestc.edu.cn, zenghui.wang@uestc.edu.cn, shpei@uestc.edu.cn)
† These authors contributed equally to this work.

 

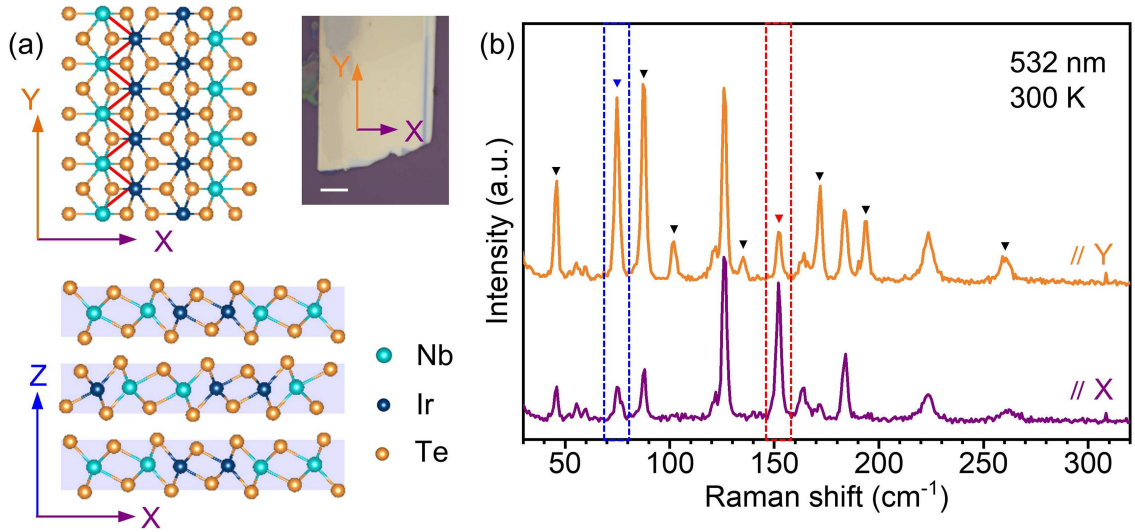


**Figure 1** (Color online) (a) Crystal structure of $NbIrTe_4$, where ($x$, $y$, $z$) represent the sample coordinates; right: optical image of the $NbIrTe_4$ flake being tested; the purple and orange arrows in the figure indicate the laser polarization directions parallel to the $x$ and $y$ axes, respectively; scale bar: 5 μm. (b) Polarized Raman measurements of the $NbIrTe_4$ flake with laser polarization directions parallel to the $x$ and $y$ axes, respectively.

polarization, incident angle, and sample orientation [14, 15]. Such improvements will offer deeper insights into Raman tensor elements and their influence on the material's vibrational dynamics [16–18].

In this work, we demonstrate experimental detection of all phonon modes of $NbIrTe_4$ using angle resolved polarization Raman spectroscopy. The spectral detection method employed in this study overcomes the limitations of traditional two-dimensional measurements, allowing us to experimentally observe two "new" phonon modes ($B_1$ and $B_2$ modes) that are only active in the out-of-plane configuration. Through analysis of angle-resolved polarization Raman spectra at different orientations, we reveal significant anisotropic differences between the in-plane and out-of-plane directions of $NbIrTe_4$, and perform a comprehensive analysis of the Raman tensor components across different orientations. Our study not only deepens the understanding of the inherent complex anisotropic properties of $NbIrTe_4$, but also provides important theoretical support for future research on the orientation dependence of materials.

## 2 Results and discussion

The crystal structure of $NbIrTe_4$ is illustrated in Figure 1(a), which features a sandwich-like structure [3, 19] and belongs to the space group $Pmn2_1$ (orthorhombic symmetry) [1]. In this arrangement, the Nb (cyan) and Ir (dark blue spheres) atoms are positioned in the middle layer, forming parallel zigzag chains along the $b$ ($y$) axis. Consequently, many of its phonon modes exhibit strong anisotropy, such as the modes marked by the triangle in Figure 1(b) which shows the results from polarized Raman measurements and reveals clear anisotropy.

To better reveal the intrinsic in-plane and out-of-plane anisotropy of $NbIrTe_4$, we develop a dedicated Raman measurement setup, which not only facilitates the adjustments of light polarization configurations (for both incoming and outgoing light signals), but also allows rotation of sample orientation along all three axes (Figure 2(a), details in Appendixes A–C). Using this custom-built setup, we analyze the angular dependence of selected Raman peaks under three different sample orientations: H, $V_X$, and $V_Y$ (defined in Figures 2(a) and (b)).

We first rotate the polarization for different sample orientations. Specifically, we measure the two $A_1$ modes (here we follow the convention that all modes measurable under such polarization configuration can be categorized as $A_1$ modes, see Supporting Information for details), $A_1^4$ (75.12 $cm^{-1}$) and $A_1^{13}$ (152.54 $cm^{-1}$). These two modes exhibit opposite angular behavior under H and $V_Y$ orientations (Figures 2(c) and (d), left and right panels), but show synchronized maxima and minima at $\theta = 0°$ and 90° under the $V_X$ orientation (Figures 2(c) and (d), center panels). Such contrast highlights the sample orientation-dependent nature of phonon anisotropy. Fitting results in Appendix D show maximum anisotropy ratios ($R = I_{max}/I_{min}$) of ∼5.58 for the H orientation ($A_1^5$ mode at 88.08 $cm^{-1}$), ∼25.82 for $V_X$ ($A_1^{14}$ mode at 163.71 $cm^{-1}$), and ∼14.67 for $V_Y$ ($A_1^{14}$ mode), quantifying the in-plane and out-of-plane optical anisotropy in low-symmetry 2D materials. In comparison with other low-symmetry materials such as $WTe_2$ and $TaIrTe_4$ (Appendix E) [20, 21], $NbIrTe_4$ shows a relatively high in-plane anisotropy ratio. Notably, its out-of-

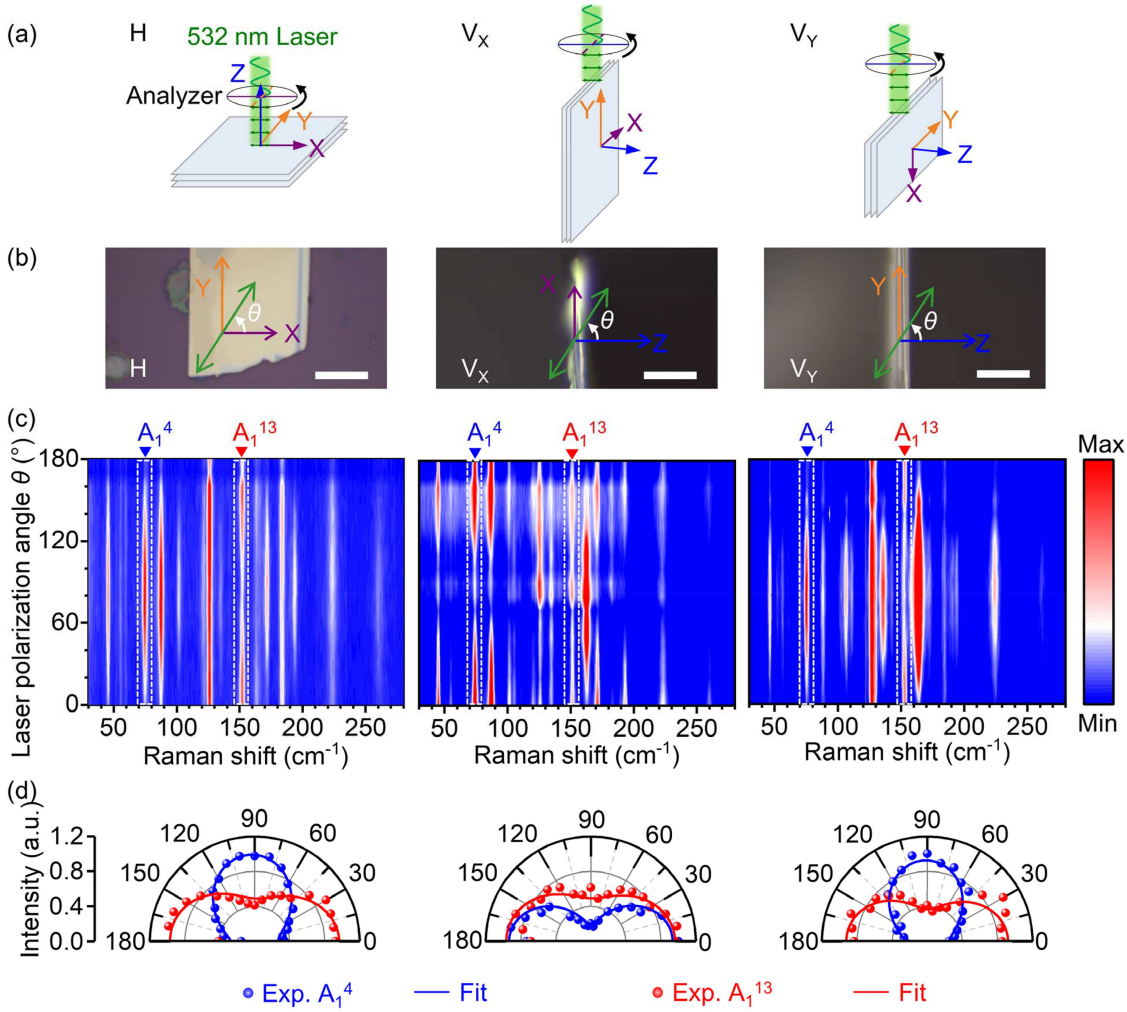


**Figure 2** (Color online) (a) Schematic of the Raman spectroscopy measurement for $NbIrTe_4$. (b) Optical images of the sample under different sample orientations, scale bar: 10 μm; where $\theta$ represents the polarization angle of the laser. (c) Polarized Raman measurements (full collection) under three different sample orientations, from left to right: H, $V_X$, and $V_Y$. (d) Relationship between the Raman intensity of the two $A_1$ modes and the angle, with spheres representing experimental data and solid lines indicating the fitting.

plane anisotropic response is substantially stronger, reflecting a distinct vibrational behavior along different sample orientations. The pronounced anisotropy is likely to be primarily governed by the intrinsic crystal symmetry [22–24], while exciton-phonon coupling [1, 9] and configuration-dependent effects [25–28] provide additional, mode-specific modulation of the observed vibrational characteristics.

To reveal a more complete picture of all the Raman-active modes in $NbIrTe_4$, we add polarizers into the signal collection path, so that the excitation and scattered light polarizations can be adjusted independently. As shown in Figures 3 and 4 distinct excitation/collection configurations across 3 sample orientations are studied, resulting in a total of 12 data sets.

We first examine the Raman spectra under polarization configurations with the excitation and scattered light polarized in parallel ("XX", "YY", and "ZZ" configurations, Figures 3(a)–(c)). As mentioned before, all modes measurable under such configurations are categorized as the $A_1$ mode (see Supporting Information for details). We identify a total of 19 $A_1$ modes. Such comprehensive data allow us to make new observations unavailable to previously reported studies [1]. Among the 19 modes, one mode ($A_1^{10}$) is detectable exclusively under the $V_X$ orientation, while three modes ($A_1^2$, $A_1^7$, $A_1^8$) are active only in the $V_Y$ orientation, as shown in Figures 3(a)–(c). These results indicate that although all these peaks belong to the $A_1$ vibrational symmetry, their intensity exhibits an observable dependence on both polarization and measurement configuration. The Raman shifts and intensities corresponding to these 19 $A_1$ modes are summarized in Appendix F. Additionally, by comparing the measurements under the three sample orientations (H, $V_X$, $V_Y$), we observe an anomalous behavior in which all $A_1$ modes exhibit the highest intensity under the $V_X$-ZZ sample orientation (Figure 3(b)) relative to the other

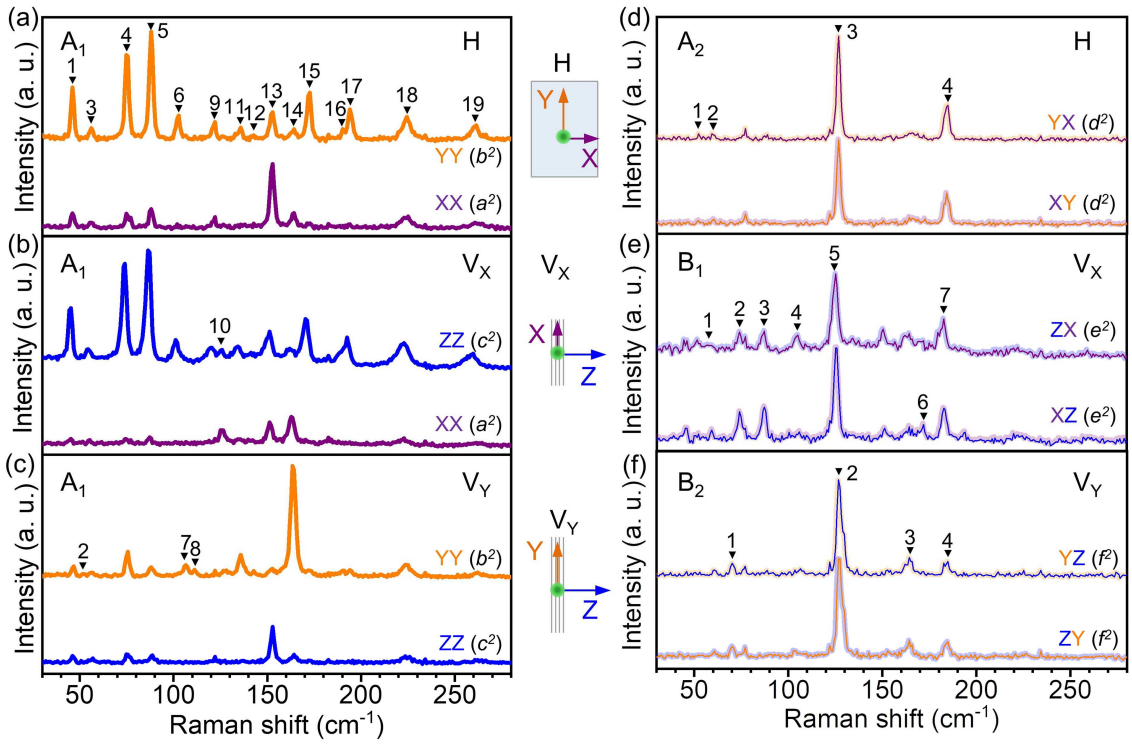


**Figure 3** (Color online) $A_1$ modes measured under three different sample orientations, (a) H, (b) $V_X$, and (c) $V_Y$. The positions of the Raman peaks are indicated by the triangles. From top to bottom, (d) $A_2$ mode observed in the H orientation, (e) $B_1$ mode detected in the $V_X$ orientation, and (f) $B_2$ mode measured in the $V_Y$ orientation, respectively. Inset: schematic diagrams of the sample orientations of H, $V_X$, and $V_Y$.

orientations, which is rarely observed in 2D Raman experiments. The observed enhancement may be attributed to several factors: (i) perturbation of Raman tensor symmetry [10, 29], where local strain, interlayer relaxation, or surface effects slightly break the ideal crystal symmetry and activate otherwise weak tensor components; (ii) resonant enhancement [1,30], whereby partial resonance with intermediate electronic states amplifies the scattering efficiency of certain phonons; and (iii) interference or multi-phonon effects [31, 32], particularly in the context of the layered structure of $NbIrTe_4$.

We next examine the Raman spectra under configurations in which the excitation and scattered light are polarized orthogonally (Figures 3(d)–(f)), in order to observe Raman vibrations other than the $A_1$ modes. Under the H orientation (Figure 3(d)), we successfully detect four $A_2$ modes (Appendix G). These four modes show no significant differences across the two polarization configurations. Overall, for the in-plane sample orientation, we identify 19 phonon modes, including 15 $A_1$ modes and 4 $A_2$ modes. When we further examine out-of-plane sample orientations $V_X$ and $V_Y$ (Figures 3(e) and (f)), the data reveal $B_1$ and $B_2$ modes of $NbIrTe_4$, which have not been observed in conventional polarization-resolved Raman studies [1]. Specifically, we measure 7 $B_1$ modes (Appendix H) and 4 $B_2$ modes (Appendix I). The experimental data reveal different configuration dependence in the intensity of the same phonon modes. For example, the intensity of all $B_2$ modes shows little variation between the two polarization configurations (well confirming the Hermitian nature of the Raman tensors), whereas some of the $B_1$ modes exhibit distinct intensity variations (revealing challenges in performing an ideal measurement). Further analysis indicates that the $B_1^4$ and $B_1^6$ modes are only active in the $V_X$-ZX and $V_X$-XZ sample orientations, respectively.

Aiming to clarify the relationship among Raman tensor elements, phonon frequencies, and experimental configurations, we conduct a theoretical analysis based on Raman selection rules. The broken inversion symmetry and 24-atom unit cell of the material give rise to 72 phonon modes, including 69 potentially Raman-active modes with irreducible representations: $\Gamma = 23A_1 + 12A_2 + 11B_1 + 23B_2$ [1]. According to classical Raman selection rules, the intensity ($I$) of Raman-active modes in anisotropic 2D materials depends on the material's intrinsic Raman tensor $R$, the incident polarization vector ($\hat{e}_i$), and the scattered polarization vector($\hat{e}_s$) [16, 33]:

$$I \propto |\hat{e}_s \cdot R \cdot \hat{e}_i|^2 .$$

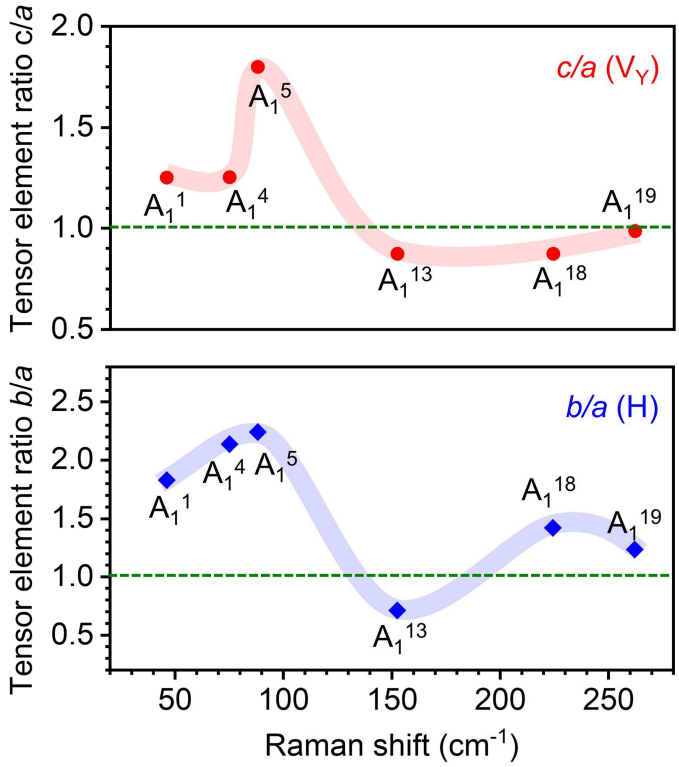


**Figure 4** (Color online) The fitted value ratios of the Raman tensor elements in 6 stable $A_1$ modes under H ($b$) and $V_Y$ ($c$) orientations. The fitting formulas under different measurement configurations are summarized in Appendix K (see Supporting information for more details).

The full 3×3 tensor of a Raman-active mode in $NbIrTe_4$ is

$$R(\mathrm{A_1}) = \begin{pmatrix} a & 0 & 0 \\ 0 & b & 0 \\ 0 & 0 & c \end{pmatrix}, \quad R(\mathrm{A_2}) = \begin{pmatrix} 0 & d & 0 \\ d & 0 & 0 \\ 0 & 0 & 0 \end{pmatrix},$$

$$R(\mathrm{B_1}) = \begin{pmatrix} 0 & 0 & e \\ 0 & 0 & 0 \\ e & 0 & 0 \end{pmatrix}, \quad R(\mathrm{B_2}) = \begin{pmatrix} 0 & 0 & 0 \\ 0 & 0 & f \\ 0 & f & 0 \end{pmatrix}.$$

In this case, the tensor elements $a$, $b$, and $d$ (uncolored) correspond to the phonon modes associated with the in-plane polarizability of the crystal, while the parameters $c$, $e$, and $f$, marked in red, reflect the changes related to the phonon modes associated with the out-of-plane polarizability of the crystal. In summary, the elements associated with distinct orientations differ from one another in value and are not equivalent in role. Consequently, the Raman peak intensities of the $NbIrTe_4$ crystal, measured at various sample orientations and polarization configurations, display notable variations.

Raman selection rule analysis (Appendix J, details in Supporting Information) shows that while the $A_1$ mode is active in all orientations, the $A_2$, $B_1$, and $B_2$ modes are orientation-specific, highlighting the pronounced anisotropy of $NbIrTe_4$: $A_2$ modes are observable only in-plane (ab plane), $B_1$ only observable in the $ac$ plane, and $B_2$ only observable in the $bc$ plane. Each mode is governed by distinct Raman tensor components ($A_1$: $a$, $b$, $c$; $A_2$: $d$; $B_1$: $e$; $B_2$: $f$), enabling precise modulation of Raman intensity through polarization, which facilitates detailed probing of crystal lographic-direction-dependent vibrational properties.

Finally, we analyze the relative values of the Raman tensor elements ($a$, $b$, $c$) for $A_1$ modes. Figure 4 shows the relative values of these Raman tensor elements ($a$, $b$, $c$), which are extracted by fitting the angular polarization Raman spectra of 6 stable $A_1$ modes under 3 different orientations, and are normalized to element $a$ (details in Supporting Information). A correlation between the relative values of Raman tensor elements and Raman shift (lattice vibration frequencies) is observed, as anticipated. Such results demonstrate that, in the Raman scattering process, the interaction between lattice vibration modes and the electromagnetic field of the incident light are

influenced by the phonon frequency [34, 35]. Furthermore, according to previous studies, this interaction is also influenced by the energy of the incident laser [36–38].

By comparing the $V_X$, and $V_Y$ orientations, we observe across different measurements a consistent trend in which the values of the Raman tensor element $c$ vary with the Raman shift (Appendix L). In addition to the overall trends, the relative contributions of individual tensor elements differ across specific peaks. For instance, the contribution of element $b$ in the H (in-plane) orientation is significantly larger than that of element $a$, whereas the contribution of element $c$ in the $V_X$ (out-of-plane) orientation surpasses that of element $a$ in the low Raman shift region and becomes comparable to it in the high Raman shift region. These observations suggest that the out-of-plane vibrational response in $NbIrTe_4$ exhibits distinct physical characteristics from the in-plane behavior, highlighting the importance of exploring out-of-plane properties in low-symmetry 2D materials.

The observations summarized in Figure 4 suggest that the influence of the Raman tensor elements on the same phonon mode is not only orientation-dependent but also frequency-dependent [39, 40]. This variation may be attributed to differences in phonon eigenvector orientations, anisotropic electron-phonon interactions, or symmetry-dependent selection rules, which influence the Raman scattering intensity under different experimental configurations [23, 41, 42]. Our finding further highlights the complexity of the material's anisotropic characteristics in different experimental configurations [43].

## 3 Conclusion

In this study, we systematically investigate the anisotropic phonon modes of 2D $NbIrTe_4$ under 3 sample orientations (H, $V_X$, and $V_Y$) using angle-resolved polarization Raman spectroscopy. In total, we identify 19 $A_1$, 4 $A_2$, 7 $B_1$, and 4 $B_2$ modes. The $B_1$ and $B_2$ modes are observed experimentally for the first time, overcoming the limitations of conventional two-dimensional polarized Raman spectroscopy. By fitting the angularly polarized Raman spectra under different measurement configurations, we determine that $NbIrTe_4$ exhibits a maximum anisotropy ratio in the out-of-plane configuration. Further, comparison across H, $V_X$, and $V_Y$ orientations reveals a consistent dependence of Raman tensor elements on phonon frequency, with tensor $c$ showing stronger contributions in out-of-plane configuration, highlighting the pronounced out-of-plane vibrational response in $NbIrTe_4$. These findings offer additional insights into the orientation-dependent optical and vibrational properties of $NbIrTe_4$, and can advance the understanding of anisotropic responses in 2D layered crystals [44]. It could be valuable for understanding and engineering physical properties that dictate the performance of polarization-sensitive, anisotropic light-emitting devices, and thermally managed nanoelectronics. Based on the experimental results presented here, future work can be carried out focusing on first-principles phonon calculations to further elucidate the microscopic origin of the observed vibrational modes, which would establish a more direct correspondence between experimental and theoretical Raman responses.

## 4 Methods

### 4.1 Preparation of $NbIrTe_4$ flakes

$NbIrTe_4$ flakes are mechanically exfoliated from bulk $NbIrTe_4$ crystals and transferred onto viscoelastic poly(dimethylsiloxane) (PDMS) stamps for angle resolved Raman measurements. The $NbIrTe_4$ flakes on PDMS (product model: PF-40-X4, the thickness is 170 μm) are then mounted onto a custom-built rotational stage (Appendixes A and B). The crystal axes $a$ and $b$ are aligned with the rotation axis of the sample to enable the detection of $V_a$ and $V_b$ in the out-of-plane orientation.

### 4.2 Angle-resolved Raman measurements

The in-situ spectroscopic studies are performed using a WITec Raman system (Appendix A) with 532 nm laser excitation. Two-notch filters centered at 532 nm, with a narrow bandwidth (5 $cm^{-1}$) and high optical density (OD $> 4$), are used to reject the Rayleigh scattering. The laser beam is focused on the sample using a 100× objective lens and the diameter of the laser spot is on the order of 1 μm (Appendix N). The laser power is set below 1 mW to avoid sample heating.

**Acknowledgements** This work was supported by National Natural Science Foundation of China (Grant Nos. T2325007, 62450003, U21A20459, 62104029), Zhejiang Provincial Natural Science Foundation of China (Grant No. ZCLQN25A0407), and Opening Project of State Key Laboratory of Metastable Materials Science and Technology (Yanshan University) (Grant No. 202504).

**Supporting information** Appendixes A–N. The supporting information is available online at info.scichina.com and link.springer.com. The supporting materials are published as submitted, without typesetting or editing. The responsibility for scientific accuracy and content remains entirely with the authors.

**References**


1 Shojaei I A, Pournia S, Le C, et al. A Raman probe of phonons and electron-phonon interactions in the Weyl semimetal $NbIrTe_4$. Sci Rep, 2021, 11: 8155
2 Chen H, Li Y, Wu H, et al. Unusual polarization and temperature-dependent Raman response in Weyl semimetal $NbIrTe_4$. Solid State Commun, 2019, 289: 56–60
3 Liu X, Lai J, Zhan J, et al. Prediction of the dual quantum spin hall insulator in the $NbIrTe_4$ monolayer. Chin Phys Lett, 2025, 42: 037302
4 Zhang J, Zhang T, Yan L, et al. Colossal room-temperature terahertz topological response in type-II Weyl SEmimetal $NbIrTe_4$. Adv Mater, 2022, 34: 2204621
5 Wen T, Li J, Zhang M, et al. Discerning the vibrational nature of $ReS_2$ Raman modes using solid-angle-resolved Raman spectroscopy. ACS Photonics, 2022, 9: 3557–3562
6 Lin M L, Leng Y C, Cong X, et al. Understanding angle-resolved polarized Raman scattering from black phosphorus at normal and oblique laser incidences. Sci Bull, 2020, 65: 1894–1900
7 Lee J E, Wang A, Chen S, et al. Spin-orbit-splitting-driven nonlinear Hall effect in $NbIrTe_4$. Nat Commun, 2024, 15: 3971
8 Xia J, Yan J, Wang Z, et al. Strong coupling and pressure engineering in $WSe_2$-$MoSe_2$ heterobilayers. Nat Phys, 2021, 17: 92–98
9 Chang Y C, Chan Y C, Das B, et al. Distinctive characteristics of exciton-phonon interactions in optically driven $MoS_2$. Phys Rev Mater, 2024, 8: 074003
10 Pimenta M A, Resende G C, Ribeiro H B, et al. Polarized Raman spectroscopy in low-symmetry 2D materials: angle-resolved experiments and complex number tensor elements. Phys Chem Chem Phys, 2021, 23: 27103–27123
11 Xia J, Li D F, Zhou J D, et al. Pressure-induced phase transition in Weyl semimetallic $WTe_2$. Small, 2017, 13: 1701887
12 Wen T, Zhang M, Li J, et al. Orientation-polarization dependence of pressure-induced Raman anomalies in anisotropic 2D $ReS_2$. Nanoscale Horiz, 2023, 8: 516–521
13 Leng Y C, Chen T, Lin M L, et al. Zenith-angle resolved polarized Raman spectroscopy of graphene. Carbon, 2022, 191: 471–476
14 Huang S, Wang C, Xie Y, et al. Optical properties and polaritons of low symmetry 2D materials. Photonics Insights, 2023, 2: R03
15 Wang F, Xu Y, Mu L, et al. Anisotropic infrared response and orientation-dependent strain-tuning of the electronic structure in $Nb_2SiTe_4$. ACS Nano, 2022, 16: 8107–8115
16 Loudon R. The Raman effect in crystals. Adv Phys, 2001, 50: 813–864
17 Pei S, Zhang Z, Jiao C, et al. Quantitative regulation of electron-phonon coupling. Rep Prog Phys, 2024, 87: 078001
18 Kranert C, Sturm C, Schmidt-Grund R, et al. Raman tensor formalism for optically anisotropic crystals. Phys Rev Lett, 2016, 116: 127401
19 Empante T A, Zhou Y, Klee V, et al. Chemical vapor deposition growth of few-layer $MoTe_2$ in the 2H, 1T′, and 1T phases: tunable properties of $MoTe_2$ films. ACS Nano, 2017, 11: 900–905
20 Kim M, Han S, Kim J H, et al. Determination of the thickness and orientation of few-layer tungsten ditelluride using polarized Raman spectroscopy. 2D Mater, 2016, 3: 034004
21 Bainsla L, Zhao B, Behera N, et al. Large out-of-plane spin-orbit torque in topological Weyl semimetal $TaIrTe_4$. Nat Commun, 2024, 15: 4649
22 Huang M, Yan H, Chen C, et al. Phonon softening and crystallographic orientation of strained graphene studied by Raman spectroscopy. Proc Natl Acad Sci USA, 2009, 106: 7304–7308
23 Benshalom N, Asher M, Jouclas R, et al. Phonon-phonon interactions in the polarization dependence of Raman scattering. J Phys Chem C, 2023, 127: 18099–18106
24 Zhang M, Jiao C, Wen T, et al. Discerning the vibrational nature of $ReS_2$ Raman modes using solid-angle-resolved Raman spectroscopy, Acta Phys Sin, 2022, 71: 140702
25 Jiao C, Pei S, Wu S, et al. Tuning and exploiting interlayer coupling in two-dimensional van der Waals heterostructures. Rep Prog Phys, 2023, 86: 114503
26 Jiao C, Pei S, Zhang Z, et al. Exploration toward a new stacking-pressure phase diagram in bilayer AA- and AB-$MoS_2$. Appl Phys Rev, 2024, 11: 031417
27 Zhang Z, Jiao C, Pei S, et al. Pressure-triggered stacking dependence of interlayer coupling in bilayer $WS_2$. Sci China-Phys Mech Astron, 2024, 67: 288211
28 Pei S, Wang Z, Xia J. Interlayer coupling: an additional degree of freedom in two-dimensional materials. ACS Nano, 2022, 16: 11498–11503
29 Zhang S, Mao N, Zhang N, et al. Anomalous polarized raman scattering and large circular intensity differential in layered triclinic $ReS_2$. ACS Nano, 2017, 11: 10366–10372
30 Moutinho M V O, Eliel G S N, Righi A, et al. Resonance Raman enhancement by the intralayer and interlayer electron-phonon processes in twisted bilayer graphene. Sci Rep, 2021, 11: 17206
31 Wang Z, Huang C Y, Hsu C H, et al. Observation of a van Hove singularity of a surface Fermi arc with prominent coupling to phonons in a Weyl semimetal. Phys Rev B, 2022, 105: 075110
32 Zacharias M, Seiler H, Caruso F, et al. Multiphonon diffuse scattering in solids from first principles: application to layered crystals and two-dimensional materials. Phys Rev B, 2021, 104: 205109

33 He C, Wang W. Bulk pentagon carbon allotrope and its properties. Comput Mater Sci, 2025, 246: 113421

34 Castro Neto A H, Guinea F. Electron-phonon coupling and Raman spectroscopy in graphene. Phys Rev B, 2007, 75: 045404

35 Zhao X, Li Z, Wu S, et al. Raman spectroscopy application in anisotropic 2D materials. Adv Elect Mater, 2024, 10: 2300610

36 Deng Z, Li Z, Wang W, et al. Vibrational properties and Raman spectra of pristine and fluorinated blue phosphorene. Phys Chem Chem Phys, 2019, 21: 1059–1066

37 Wen M, Chen X, Zheng Z, et al. In-plane anisotropic Raman spectroscopy of van der Waals $\alpha$-$MoO_3$. J Phys Chem C, 2020, 125: 765–773

38 Jin M, Zheng W, Ding Y, et al. Raman tensor of $WSe_2$ via angle-resolved polarized Raman spectroscopy. J Phys Chem C, 2019, 123: 29337–29342

39 Wen T, Li J, Deng Q, et al. Analyzing anisotropy in 2D rhenium disulfide using dichromatic polarized reflectance. Small, 2022, 18: 2108028

40 Wang C, Yang X, Ma Y, et al. Microstructure and photoluminescence of ZnO: Cd nanorods synthesized by hydrothermal method. Acta Phys Sin, 2014, 63: 157701

41 Zhang S, Huang J, Yu Y, et al. Quantum interference directed chiral raman scattering in two-dimensional enantiomers. Nat Commun, 2022, 13: 1254

42 Tesar K, Gregora I, Beresova P, et al. Raman scattering yields cubic crystal grain orientation. Sci Rep, 2019, 9: 9385

43 Xu B, Zhu J, Xiao F, et al. Identifying, resolving, and quantifying anisotropy in $ReS_2$ nanomechanical resonators. Small, 2023, 19: 2300631

44 Qiu H, Yu Z H, Zhao T G, et al. Two-dimensional materials for future information technology: status and prospects. Sci China Inf Sci, 2024, 67: 160400